

advances.sciencemag.org/cgi/content/full/6/48/eabd1313/DC1

**Supplementary Materials for
The arches of chaos in the Solar System**

Nataša Todorović*, Di Wu, Aaron J. Rosengren

*Corresponding author. Email: ntodorovic@aob.rs

Published 25 November 2020, *Sci. Adv.* **6**, eabd1313 (2020)
DOI: 10.1126/sciadv.abd1313

The PDF file includes:

Supplementary Materials and Methods
Supplementary Text
Figs. S1 to S3
Tables S1 and S2
Legends for movies S1 to S3

Other Supplementary Material for this manuscript includes the following:

(available at advances.sciencemag.org/cgi/content/full/6/48/eabd1313/DC1)

Movies S1 to S3

Materials and Methods

Numerical Methods

The results of this study relied on two well-established, open source, N -body orbit integrators, ORBIT9 (29) and REBOUND (30). In particular, ORBIT9 was used in the computation of the fast-Lyapunov indicator (FLI) maps (Fig. 1); while the **Mercurius** package within REBOUND, being specifically designed for accurate close-encounter and collisional dynamics, was used for the Jovian-minimum-distance maps (Figs. 2-4) and subsequent simulations (fig. S3; movies S1-S3). The dynamical models employed contain the seven major planets (from Venus to Neptune) as perturbers or Jupiter as the only perturber, both in realistic N -body simulations as opposed to simple mathematical models like the planar, circular, and restricted three-body problem (PCR3BP).

One approach to visualizing phase-space structures in systems of more than two degrees of freedom relies on the computation of the fast-Lyapunov indicator (FLI) over sets of initial conditions of interest (21-26). Writing the first-order differential equations defining the dynamics of the (test particle) TP, $\dot{x} = f(x, t)$, where $x = (r, v)$ is the state vector of the Cartesian components of the position r and velocity v in a heliocentric reference frame, the variational equations can be stated from the Jacobian matrix as $\dot{w} = [\partial f / \partial x(x, t)]w$. The FLI follows from the variational system and reflects the growth of the tangent vector w in some fixed time t by $FLI_t(x, w) = \sup_{\tau \leq t} \log |w(\tau)|$. For chaotic orbits, the FLI will grow faster than for stable ones, enabling a quick distinction between them (20). Various dynamical regimes, including orbital resonances, can be distinguished by monitoring time histories of the FLI. Here, we compute the FLI for refined grids of initial conditions over very short timescales (Fig. 1) to capture traces of the manifolds of hyperbolic trajectories (25-27).

To drastically reduce the computational burden, past studies have relied on the calculation of more practical, though less rigorous, quantities of interest, such as the maximum eccentricity reached by an orbit during its evolution or the collisional or scattering timescale (12-18), which otherwise do not require the simultaneous integration of the variational system. We have correlated the structures in the FLI map with close approaches to Jupiter through the computation of Jovian-minimum-distance maps (Figs. 2-4). This permitted us to cover a much broader range of three-body energies than previously considered, which, hitherto, have largely been limited to the ‘bottlenecks’ about L_1 and L_2 (2, 3, 9–11, 27); but also somewhat precludes the possibility of easily identifying the exact homoclinic-heteroclinic connections responsible for all foliated substructure. In Figs. 2-4 and movie S1, we monitor the distance between Jupiter and the TPs during their 100-year evolution and record the minimum values in units of planetary radii. The colorbar then represents the logarithm of the minimum approach distance, such that a value of less than 2.87 means that the TP entered the Jovian Hill sphere with 0 corresponding to a Jovian impact, and a value above 3.35 implies it never got within 3 Hill radii.

Auxiliary Data

Our results relied on data obtained from NASA’s JPL/Horizons service (35).

Supplementary Text

Nomenclature

The PCR3BP refers to the idealized dynamical model that consists of a massless TP and two massive bodies (e.g., Jupiter and the Sun) moving in circular orbits about their common center of mass, with all bodies moving in the same plane. The Sun-Jupiter Lagrange points are the five stationary solutions or equilibria in the PCR3BP, where L_1 , L_2 , and L_3 lie along a line joining the Sun and Jupiter, and L_4 and L_5 form equilateral triangles with them (see fig. S1). Jupiter's Hill sphere is the region between diametrically opposite Lagrange points L_1 and L_2 , in which the motion of the TP is dominated by the attraction of Jupiter. A vast and hardly surveyable literature exists on the study of the PCR3BP (1-4, 6-9, 25) and a hierarchy of more realistic, and more complicated, models, e.g., the elliptic orbit of the massive bodies (22), three-dimensional motion of the TP (5, 10, 11, 27). In our N -body simulations, all of these additional complications and more are inherently taken into account.

Associated with the collinear Lagrange points, or their dynamical extensions to periodic or quasi-periodic orbits, are stable and unstable manifolds, certain phase-space structures that asymptotically approach or depart the Lagrange points (or their dynamical extensions). The periodic orbits most often treated in the literature (1-4, 6-9), the Lyapunov orbits, reside in the bottlenecks that partitions the interior and exterior Hill's regions. Figure S2 shows an illustration of such Lyapunov orbits about L_1 and L_2 , and their associated stable and unstable manifold tubes that structure the phase space and provide a conduit for particles traveling to and from Jupiter. A homoclinic orbit is the intersection between a stable and unstable manifold of the same equilibrium point, or periodic/quasi-periodic orbit; while a heteroclinic orbit is the intersection of such manifolds from two different invariant objects. The underlying homoclinic-heteroclinic structures allow one to classify and organize distinctly different types of global motions of the PCR3BP in terms of their relation to the equilibrium points (1).

Also connected with any three-body problem model is orbital resonances, which are commensurabilities amongst the frequencies of orbital motions (2, 4, 12, 13, 16-18, 22-24); the most studied of which are known as mean-motion resonances (MMRs) involving integer ratios of orbital periods. The vicinity interior and exterior to Jupiter where first-order MMRs overlap is known as the planetary chaotic zone (12, 13), in which the timescales for scattering are some thousands of orbital periods for the strongest regions.

In the PCR3BP, the Tisserand parameter with respect to Jupiter is defined as $T_j = a_j/a + 2\sqrt{(1-e^2)a/a_j} \cos i$, where $a_j = 5.2$ AU is Jupiter's semi-major axis (17, 34). It is an approximation to the Jacobi constant, which is an integral of the motion in the PCR3BP, and is used to distinguish among, e.g., Halley-family comets or Damocloids ($T_j \leq 2$), JFCs ($2 < T_j \leq 3$), and asteroids ($T_j > 3$).

Placing results in context of the PCR3BP

Figure 3 portrayed a highly resolved image of the uncovered structures, along with callouts to specific evolutions in Cartesian inertial-frame coordinates of several initial conditions located on the stable manifolds. Additional context for our results is given in fig. S3, which shows example trajectories taken from the map and projected into the Sun-Jupiter rotating frame. Such evolutions exhibit a complicated array of behaviors, characteristic of manifold dynamics.

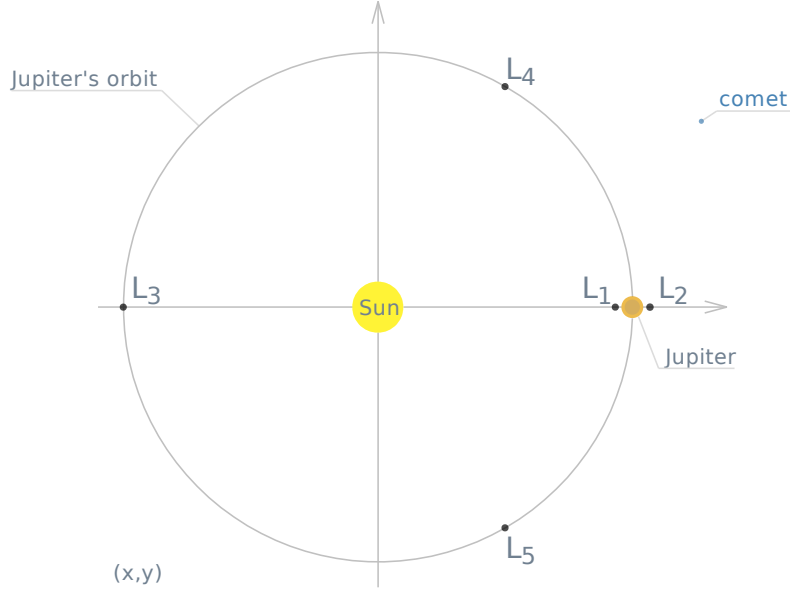


Figure S1. Location of the five Lagrange equilibrium points for the PCR3BP in the Sun-Jupiter system

The collinear points, L_1 , L_2 , and L_3 , which lie along the straight line joining the Sun and Jupiter, are unstable stationary solutions, while the equilateral points, L_4 and L_5 , which lead or trail Jupiter in its orbit by an angular distance of 60° , are stable equilibria. In each equilibrium case, the three bodies are at rest when viewed in a coordinate system that rotates at constant angular velocity about their barycenter. Given at a certain time both the position (x, y) and velocity (\dot{x}, \dot{y}) of a small Solar System body (e.g., comet), it is generally impossible to predict for any arbitrary time interval the future progress of its motion. Nevertheless, the invariant manifold structures provide the framework for understanding many complex dynamical phenomena within the PCR3BP.

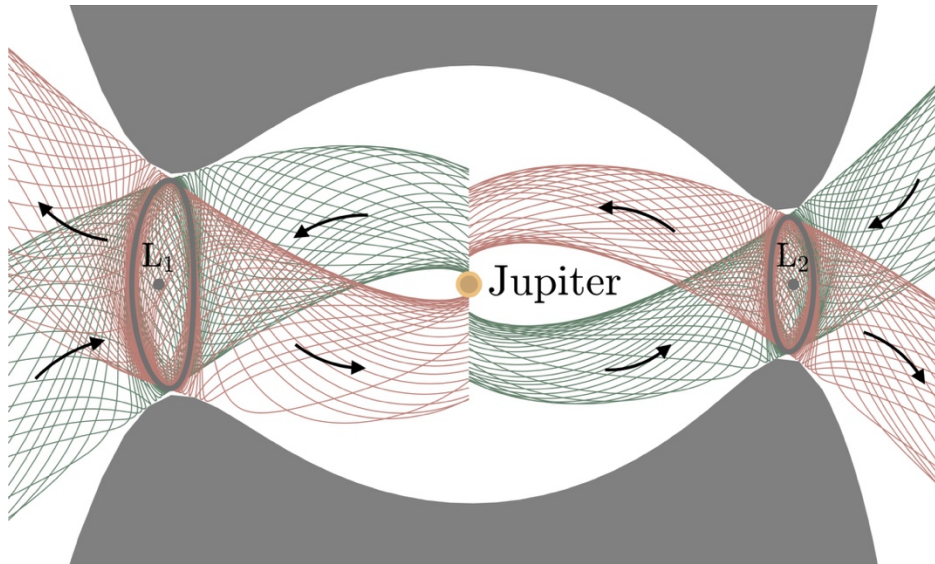


Figure S2. The stable and unstable invariant manifold tubes associated with Lyapunov orbits around L_1 and L_2 governing flow near Jupiter

The stable (*green, black arrows* pointing towards the periodic orbit) and unstable (*red, black arrows* pointing away from the periodic orbit) manifolds associated to Lyapunov orbits around the collinear Lagrange points. The energetically forbidden zone is *gray* and Hill's region contains bottlenecks about L_1 and L_2 . Transition between the interior and exterior realms, scattering, temporary capture, and collision are conditioned by such invariant manifold structures.

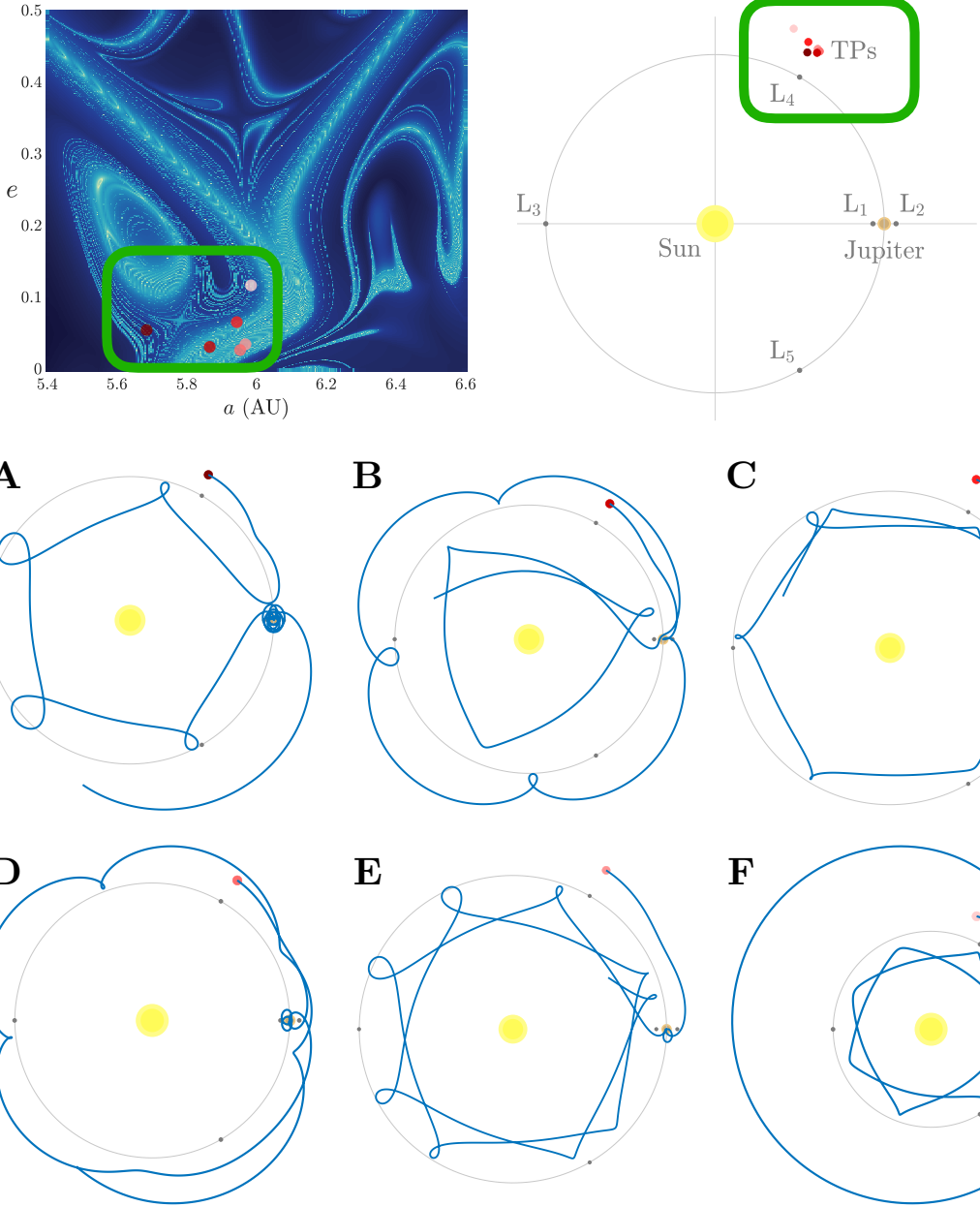


Figure S3. Example evolutionary states in the Sun-Jupiter rotating frame of initial conditions located on the uncovered manifold structures

Superimposed on stability map of Fig. 3 (*top left*) and PCR3BP rotating frame (*top right*) are the initial conditions whose trajectories are further illustrated in panels A-F. These example trajectories are integrated for 100 years with the same dynamical model used to produce the map, and then projected into the Sun-Jupiter rotating frame to highlight their relationship with the Lagrange points. All six trajectories experience a close encounter with Jupiter after only one or two orbital revolutions around the Sun. Five of them (A-C, E, F) transit through the Jupiter's Hill region, while the orbit in panel D stays on the same side of Jupiter after the close encounter.

Table S1. Orbital elements used for the numerical experiments

Relevant Heliocentric-ecliptic orbital elements of Jupiter (in degrees) at the simulation epoch 30 September 2012, obtained from JPL/Horizons (33), used to setup the numerical experiments in Figs. 1-3 and movies S1-S3.

Inclination	Argument of perihelion	Longitude of ascending node	Mean anomaly
1.304095433921203E+00	2.738332953159384E+02	1.005051860216016E+02	4.684213694231330E+01

Table S2. Orbital elements of Jupiter-family comet, Oterma

Heliocentric-ecliptic orbital elements of 39P/Oterma at the epochs 1 January 1910 and 8 April 1943, obtained from JPL/Horizons (33), used to setup the numerical experiments in Fig. 4.

	1 January 1910	8 April 1943
Semi-major axis (AU)	6.925850692714088E+00	3.961516742172333E+00
Eccentricity	1.594266713982173E-01	1.444995136733259E-01
Inclination (°)	3.077926672793472E+00	3.983867699367722E+00
Argument of perihelion (°)	2.411079586498954E+02	3.547675772449415E+02
Longitude of ascending node (°)	3.588772360504517E+01	1.558388364391905E+02
Mean anomaly (°)	1.823901134362004E+02	2.869487026767107E+01

Movie S1. Global appearance of space manifolds in one century

Jovian-minimum-distance maps computed over roughly ten orbital revolutions of Jupiter with each frame of the animation showing how the arches and foliated substructure manifest over three-year increments (Fig. 1 and 2). Each map samples four million initial values of semi-major axis and eccentricity, where the initial inclination, argument of perihelion, and longitude of ascending node of the TPs are set equal to that of Jupiter at the initial epoch 30 September 2012 (table S1). The initial mean anomaly of the TPs is set to 60° ahead of Jupiter in its orbit to reflect the Greek L_4 configuration. Two contours of Sun-Jupiter-TP three-body energy are superimposed, with -1.5194 corresponding to the value of the L_1 Lagrange point. The map covers the inner edge of the main asteroid belt at 2 AU to just beyond the semi-major axis of Uranus at 20 AU. The **Mercurius** package within REBOUND (30) was used under the Sun-Jupiter-TP three-body model.

Movie S2. Small bodies located on manifolds that lead to rapid collision with Jupiter

Heliocentric-ecliptic inertial frame evolution of the 31 colliding TPs of Fig. 3. The fastest collision occurred in just over seven years and the average collision time was roughly 36 years.

Movie S3. Small bodies located on manifolds that lead to fast escape from the Solar System

Heliocentric-ecliptic inertial frame evolution of a subset of 38 escaping TPs of Fig. 3. These elliptic-to-hyperbolic transitioning orbits reach the distances of Uranus and Neptune in roughly 38 and 44 years on average, respectively, and 63% of them get kicked to 100 AU over the course of a century.